RSC Advances

PAPER

Cite this: *RSC Adv.*, 2015, **5**, 69765

pH-dependent size and structural transition in P123 micelle induced gold nanoparticles

P. Chatterjee and S. Hazra*

Received 23rd June 2015
Accepted 31st July 2015

DOI: 10.1039/c5ra12090j

www.rsc.org/advances

The influence of the pH value of an aqueous solution of P123 micelles on the growth and formation of gold nanoparticles (AuNPs), which is of immense importance for their controlled growth in a simple, single-step synthesis process, was investigated using time-evolution optical absorption spectroscopy, dynamic light scattering and transmission electron microscopy techniques. The sizes and structures of the AuNPs are found to be pH-dependent, even within the basic region, with a transition near pH $\approx$ 9.5, though the free P123 micelles remain almost unchanged. Below this pH value, the slow reduction rate of the gold ions creates a lower number of nucleation centers, which, through an autocatalytic thermodynamically controlled reduction (ATCR), initially formed chain-like aggregated small AuNPs (of different chain lengths) and subsequently, through further diffusion and coalescence, formed well-faceted near symmetrical large AuNPs of size $\gg$19 nm, the size of the free P123 micelles. Above this pH value, the fast reduction rate of the gold ions creates a large number of nucleation centers, the growth of which is restricted by the limited amount of available gold ions for the ATCR and also by the metal–polymer hydrophobic and polymer–water hydrophilic interactions. Accordingly, controlled growth of the majority of the centers takes place through ATCR, diffusion and early capping with near individual micelles to form isolated symmetric small AuNPs of size <19 nm, with a narrow size distribution, which are desirable for different applications and fundamental studies. However, a minority (but not insignificant amount) of the centers still remain in very small sizes and are trapped inside large micellar assemblies or even in the near atomic states, which limit the yield of the isolated small AuNPs.

1 Introduction

Metal nano-objects are attracting significant attention because of their fascinating size-dependent optical, magnetic, electronic, and catalytic properties. Among them, gold nanoparticles (AuNPs) with desirable structures and functions are of special interest due to their various applications in photonics, sensors, catalysis and biomedicine.[1–12] Reduction, nucleation, stabilization and dispersion are the major steps for the synthesis of metal nanoparticles with desirable structures, morphologies (sizes and shapes) and functions. Stabilization and dispersion of AuNPs are achieved by covering them with different macromolecules such as polymers, surfactants and proteins through various interactions like covalent bonds, hydrogen bonds, electrostatic forces, and so forth.[2–5,7–11]

AuNPs are generally synthesized using the solution-phase method by chemical reduction of precursor gold ions involving organic solvents and these are then chemically attached to organic molecules that counterbalance the van der Waals attraction occurring between the nanoparticles.[5,11,13] Such AuNPs are difficult to disperse in water, which is sometimes a hindrance for further surface modification and functionalization, which is essential for particular applications. Compared to such a synthesis process, another environmentally friendly method, where AuNPs can be synthesized in aqueous media from the chemical reduction of gold ions by reducing agents such as citric acid and ascorbic acid in the presence of one or more water-soluble polymers or surfactants as capping agents, and with the support of externally supplied energy like photoirradiation, ultrasound irradiation, or heating, was developed.[5,11,14–16] In this process the colloidal stability of the nanoparticles is mainly achieved *via* the chemical binding of ligands at the surface. Such binding may again alter the intended properties of the nanoparticles.

To maintain the intended properties of the nanomaterials, lots of work is going on to develop simple, versatile and economically viable methods for the preparation of AuNPs in a size- and shape-controlled manner where the ligands (like surfactants and macromolecules) adsorb physically over the surface of the nanoparticles. In this direction, various attempts have been made to synthesize stable AuNPs at ambient temperature in a single step process from aqueous solutions of gold salts using a water-soluble triblock copolymer (TBP) which acts as both a reducing and stabilizing agent due to its amphiphilic nature.[5,12,17–21] TBPs belong to a special category of

Saha Institute of Nuclear Physics, 1/AF Bidhannagar, Kolkata 700064, India. E-mail: satyajit.hazra@saha.ac.in

nonionic surfactants which have two or more different monomers linked by covalent bonds. The most widely used TBPs are poly(ethylene oxide)–poly(propylene oxide)–poly(ethylene oxide) (PEO–PPO–PEO with the commercial name Pluronics) with different numbers of PEO and PPO blocks. In aqueous solution, TBPs form micelles with hydrophobic PPO as the core and hydrophilic PEO as the corona.[12,19–24] The corona is in the form of a surface cavity which is in direct contact with the aqueous solution and constitutes the micelle–solution interface of a TBP micelle. TBPs are mainly used to synthesize AuNPs because of their ability to reduce gold ions following the three steps: (i) reduction of gold ions in the surface cavity of TBP micelles in the solution and formation of gold clusters, (ii) adsorption of micelles on gold clusters and reduction of gold ions on the surfaces of these gold clusters, and (iii) growth of gold particles in steps and finally their stabilization by TBP micelles.[17,18,25] So any change in the micelle environment (namely the ratio of PEO and PPO block lengths, molecular weight of TBP, concentration of TBP and/or Au salt in the solution, temperature of the mixed solution, *etc.*) is expected to cause a significant change in the reduction, growth, morphology and also stabilization of the nanoparticles.

Recently, researchers have paid attention to revealing the influence of different parameters of TBP micelles on the formation and growth mechanism of AuNPs.[19–21,26] One such important parameter is the pH value of the aqueous TBP micellar solution, which is relatively less studied.[26] It was found that in a low pH region the reduction of gold ions is very slow, which results in the formation of unstable large, aggregated nanoparticles of various shapes, whereas with an increase of the pH value of the micellar solution, the reduction process of the gold ions is accelerated and highly stabilized nanoparticles with small average diameters and a narrow size distribution are formed,[26] which is contrary to other processes where reducing reagents, such as sodium citrate or ascorbic acid, are utilized.[2,27] It is clear from different studies that the pH value strongly influences the reaction kinetics. However, the exact influence of the pH value of the micellar solution on the growth kinetics of nanoparticles, understanding of which is essential for better control of the growth, size, shape, stability and amount of nanoparticles, is not very clear.

In this paper, we have tried to understand the role of the pH value of the TBP micellar solution on the simultaneous reduction of gold ions and the formation of AuNPs using complementary techniques. For this, the evolution and final state of the mixed aqueous solution, containing TBP and the gold salt, of different pH values, were monitored using ultraviolet-visible (UV-vis) spectroscopy[28–37] and dynamic light scattering (DLS)[37–39] techniques, respectively, while the morphology of the AuNPs and aggregates in the final states were imaged through transmission electron microscopy (TEM).[40] The presence of isolated large AuNPs and large micelles loaded with small AuNPs is clearly evident. The size of the isolated AuNPs decreases as the pH of the solution varies from normal to high, with a transition near pH $\approx$ 9.5. Below this value the size is much greater than that of the micelles, while above this value the size is less than that of the micelles. Also, a strong shift in the peak at 325 nm, originating from the LMCT band between the $AuCl_4^-$ ions and PEO surface cavities, has been observed. An attempt has been made to correlate these interesting observations.

2 Experimental details

2.1 Materials

Pluronic TBP, P123 [$HO(CH_2CH_2O)_{20}(CH_2CH(CH_3)O)_{70}(CH_2CH_2O)_{20}H$, $M_w = 5800$], and the gold salt, hydrogen tetrachloroaurate(III) trihydrate [$HAuCl_4 \cdot 3H_2O$], were purchased from Sigma-Aldrich and were used without further purification. MilliQ water was used as the solvent for all solution preparations and sodium hydroxide [NaOH, Merck, 35%] was used to change the pH value of the solution.

2.2 Preparations

AuNPs were prepared from a mixed aqueous solution of TBP and the gold salt at room temperature by the method developed by Sakai *et al.*[17,18,25] As a first step, an aqueous P123 solution with a concentration of 5.75 mM (3.33% w/v) was prepared by magnetic stirring for 2 h and then an aqueous $HAuCl_4$ solution with a concentration of 2 mM was prepared. It is to be noted that during the synthesis of the AuNPs, the concentrations of the gold salt and P123 in the aqueous solutions were kept fixed, and only the pH value of the P123 solution was varied within the basic region. The pH value of the as-prepared aqueous P123 solution was 6.82. By adding different amounts of NaOH solution, the pH value of the P123 solution was varied (8.26, 9.50, 10.60, 11.18 and 11.58) and measured using a pH meter. Finally, 45 ml of P123 solutions of different pH values were mixed separately with 5 ml of $HAuCl_4$ solution and stirred for about 10 min. Then the mixed solutions were kept under ambient conditions ($\sim$25 °C and $\sim$40%) for 3 h without any disturbance. The color of the solutions changed from colorless to pink-purple or purple within half an hour and remained the same thereafter in most cases. The pH values reported in this paper are those of the aqueous P123 solutions before mixing with the aqueous $HAuCl_4$ solution. The mixed solutions and P123 solutions of pH 6.82, 8.26, 9.50, 10.60, 11.18 and 11.58 are henceforth referred to as pH $\approx$ 6.8, 8.3, 9.5, 10.6, 11.2 and 11.6, respectively.

2.3 Characterization

DLS experiments were performed to probe the size variation of the micelles in the pure aqueous P123 solutions with different pH values before and after addition of the aqueous $HAuCl_4$ solution. Also, an idea about the size of the nanostructures formed by the AuNPs and P123 micelles in the mixed solutions was obtained from DLS measurements. The measurements were carried out using a Zetasizer (Nano-S, Malvern Instrument).[37] The light source was He–Ne laser operated at 633 nm with a maximum output power of 15 mW. Each measurement was repeated at least two times.

Time dependent UV-vis absorption spectra of the mixed solutions of $HAuCl_4$ + P123 + water were carried out with a UV-

vis spectrophotometer (Lambda 750, PerkinElmer).[36,37] For comparison UV-vis absorption spectra of the mixed solutions of P123 + water were also obtained. The instrument was operated in spectrum mode with a wavelength interval of 1 nm and the samples were held in quartz cuvettes with a path length of 1 cm. It makes use of a tungsten halogen lamp as the visible light source and a deuterium discharge lamp for the UV light source. Surface plasmon resonance (SPR) band determination of the AuNPs[30,31] is one of the most familiar applications of this technique. SPR arises due to the resonance between the incident radiation and collective oscillation of conducting electrons of metal nanostructures.

The sizes and morphologies of the nanostructures composed of AuNPs and P123 micelles were observed using TEM (Tecnai S-twin, FEI or JEM 2100 HR, JEOL), operating at an accelerating voltage of 200 kV. Prior to the TEM sample preparation, the solutions were centrifuged with water at 12 000 rpm for 20 min to remove the free P123 micelles from the solutions as much as possible. Samples were then prepared by placing a drop of gold colloids on a carbon-coated copper grid and allowed to dry in air. It should be noted that no staining agent, which is usually employed to clearly observe micellar assemblies in order to achieve an appropriate contrast against the bright background, has been used in the present study. TEM micrographs were analyzed using ImageJ software.

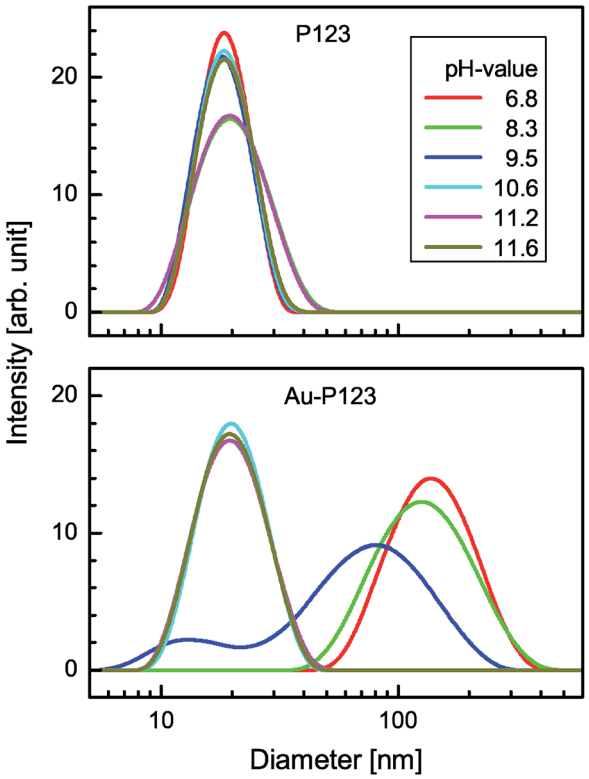

Fig. 1 Size distribution plots, obtained from DLS data, for the mixed binary (P123 + water) and ternary ($HAuCl_4$ + P123 + water) solutions of different pH values (data taken after 3 h of mixing).

3 Results and discussion

3.1 Dynamic light scattering

The particle size distribution plots, obtained from DLS measurements for all the mixed solutions after 3 h of mixing, are shown in Fig. 1. A single Gaussian-like peak with a narrow intensity size distribution and at similar position is found for all the P123 micelle solutions, suggesting there is not much variation in the size of the spherical shaped micelles with the pH value of the aqueous solution. The average hydrodynamic diameter of the P123 micelles is found to be about 19 nm, which is consistent with the value observed before at normal pH.[24]

The intensity-size or particle size distribution curve becomes highly pH-dependent when $HAuCl_4$ is added to the P123 micellar solution. Such a distribution can be categorized into three pH regions. Region 1, for pH $\approx$ 6.8 and 8.3, where a single peak with a large value (around 140 and 125 nm, respectively) is observed in the intensity size distribution curves. Region 2, for a pH value around 9.5, where dual peaks at around 13 and 80 nm are found in the intensity size distribution curve; and finally region 3, for pH values above 9.5, where a single peak at around 19 nm, similar to that of the free micelles, is found in the intensity size distribution curves. This suggests that although there is not much influence of the pH value on the sizes and shapes of the free micelles in aqueous solution, it has a strong influence on the sizes and shapes of the nanostructures that are formed when the $HAuCl_4$ solution is added into the micellar solution. The average hydrodynamic diameters ($2R_{DLS}$) that are observed for different pH values are tabulated in Table 1. In region 1, no peak corresponding to the size of the free micelles is observed. A single peak due to a large sized structure may originate from the self-aggregation of the P123 micelles due to loading of AuNPs into the surface cavities or may be due to the formation of large AuNPs or agglomeration of small AuNPs. As the pH value increases, the size of such nanostructures decreases. Also the intensity of the peak decreases, while its width increases, suggesting the formation of smaller sized nanostructures or aggregates with a larger size distribution when the pH value increases. In region 2, a new peak at around 13 nm is formed along with a decreasing intensity and increasing size distribution of the peak at around 80 nm. The appearance of the new peak is likely to originate from free AuNPs. In region 3, the peak corresponding to the large sized nanostructures or aggregates disappears completely. Instead, only a strong peak near 19 nm is observed (the width of the peak is quite narrow but wider compared to the free micelles), which is probably related to the P123-capped AuNPs. Thus the DLS measurements indicate that at high pH values, a large number of small-sized (of about 19 nm) P123-coated AuNPs are formed. The information obtained from the DLS measurements allows us to predict the possible sizes of the nanostructures formed in different solutions, which is important. However, to know the detailed growth mechanism of AuNPs in solution and their final shape and size distributions, analysis of the time evolved UV-vis spectra and TEM images is very important and is presented next.

3.2 UV-vis spectroscopy

The UV-vis absorption spectra of the mixed solutions, collected after 3 h of mixing, are shown in Fig. 2. Two peaks are observed

Table 1 Parameters such as the average hydrodynamic diameter ($2R_{DLS}$), the SPR peak position (λ_{SPR}) and its saturation intensity ($I_{SPR,s}$, relative to the intensity at 460 nm), the critical growth time (τ) and the average size ($2R_{TEM}$) of the AuNPs prepared using P123 micellar solutions of different pH values as obtained from DLS, optical absorption and TEM measurements

pH-value	$2R_{DLS}$ (nm)	λ_{SPR} (nm)	$I_{SPR,s}$ (a.u.)	τ (min)	$2R_{TEM}$ (nm)
6.8	140	564	0.27	90	49
8.3	120	557	0.34	60	—
9.5	13 & 80	538	0.38	50	4 & 16
10.6	19	531	0.15	40	4 & 14
11.2	19	529	0.15	35	—
11.6	19	525	0.19	30	4 & 11

in the mixed binary (P123 + water) solutions of different pH values, while several peaks are observed in the UV-vis spectra of the mixed ternary ($HAuCl_4$ + P123 + water) solutions of different pH values. For the mixed binary solutions, saturation in the absorption intensity below 205–208 nm and the presence of a low intensity peak or shoulder near 280 nm are observed. The intensities and positions of the strong and weak peaks near 205 and 280 nm, respectively, which arise due to P123,[26] are found to be the same for all pH values. This suggests that, though the environment of the micelles is modified by adding different amounts of NaOH to the solution, the intrinsic property of the P123 as well as the size of the micelles (as observed from the DLS study) do not alter much.

The peaks are mainly found near 205, 226, 284, 325 and 540 nm in the mixed ternary solutions (see Fig. 2). The intensities of these, however, vary with the pH value. The peaks near 205 and 284 nm are similar to those of the bare micellar solutions and thus can be assigned to the P123. The intensity of the peak near 205 nm is very high (above the saturation value) for all the solutions and thus can not be compared. The peak near 284 nm, on the other hand, becomes prominent or sharp with the increasing pH value up to a value of pH ≈ 10.6, after which it almost disappears. Peaks around 226 and 325 nm are found for the ligand-to-metal charge transfer (LMCT) transitions in $AuCl_4^-$ ions and LMCT complexes. The latter are reported to form due to the interaction of $AuCl_4^-$ ions with the PEO chains of the surface cavity.[26,27,41,42] The signatures of the peaks at 226 and 325 nm are prominent in the mixed solution of pH ≈ 6.8. Both the peaks become weak and gradually disappear with the increase of pH. Instead, a new peak near 365 nm gradually appears, which is quite prominent for a high pH. This band may arise due to the reduction in the energy gap of the $2e_u(\pi) \rightarrow 2b_{1g}(\sigma^*)$ orbitals caused by complexation of the π-donor oxygen lone pairs of the PEO parts.[6,43] The peak near 540 nm corresponds to the well-known surface plasmon resonance (SPR) of AuNPs. The position (λ_{SPR}), intensity (I_{SPR}), width and shape of this peak vary with the pH value. The values of λ_{SPR} for different pH values are tabulated in Table 1. The variations of λ_{SPR} and I_{SPR} with the pH value are shown in the inset of Fig. 2. The peak is blue shifted gradually (from 565 to 525 nm), with a large change near pH ≈ 9.5, while the intensity of the peak first increases up to pH ≈ 9.5, then decreases suddenly and again increases with increasing pH value. Thus a transition in the SPR peak, similar to that of the size distribution (obtained from DLS study), is observed near pH ≈ 9.5. The blue shift of the SPR peak with the variation in the pH value is associated with the decrease in the particle size. The width and shape of the SPR peak are found to be broad and asymmetrical for low pH values. It is known that the longitudinal component of the SPR can arise at higher wavelengths, due to the anisotropic shape or chain-like aggregation of particles. However, for the anisotropic-shaped particles, the intensity of the longitudinal component must be high compared to the transverse component, which is not the case. Thus the observed broad asymmetric SPR peak could be due to the large size distribution or chain-like aggregation of particles. The shape of the peak becomes more symmetrical with the increase of pH value, while the width of the peak decreases considerably up to pH ≈ 9.5

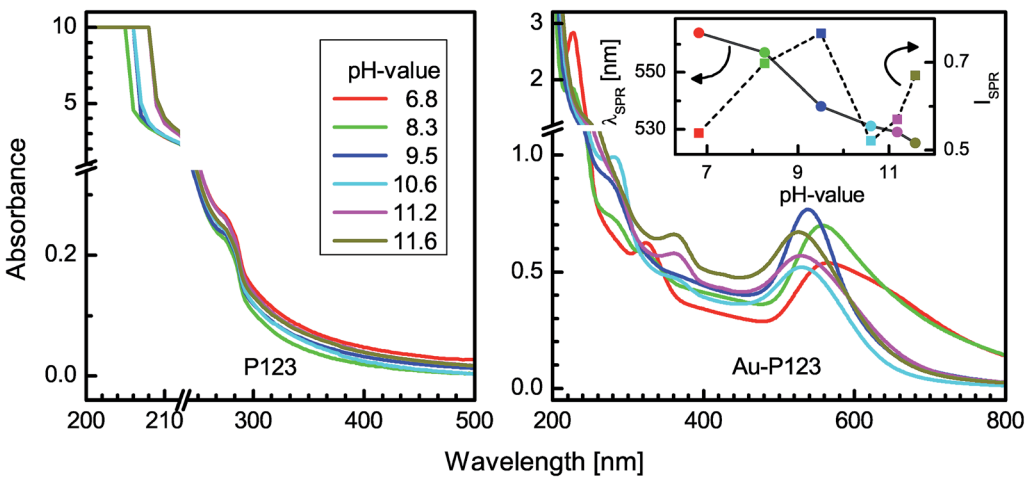

Fig. 2 UV-vis absorption spectra of the mixed binary (P123 + water) and ternary ($HAuCl_4$ + P123 + water) solutions of different pH values (data taken after 3 h of mixing). Inset: variation of the SPR peak position (λ_{SPR}) and its intensity (I_{SPR}) with pH value.

and then increases slightly above this pH value when the shape becomes almost symmetrical. The symmetrical shape of the peak is associated with a narrow size distribution and less aggregation of particles, while the slight increase of the symmetrical peak width at higher pH values is again associated with the decrease in the particle size.

The time-evolution UV-vis absorption spectra of the mixed ternary solutions, collected for different pH values, are shown in Fig. 3 to demonstrate the influence of the pH value of the aqueous solution of P123 micelles on the growth of AuNPs with time. Saturation in the intensity is observed below 205 nm for all spectra. Also, a peak near 226 nm, which decreases with time and increasing pH value, is found strong for solutions with low pH values at the initial stages, due to $AuCl_4^-$ ions. On the other hand, the SPR peak near λ_{SPR}, due to the formation of AuNPs, evolved with time. This peak is found to be very broad and asymmetric for the low pH value solutions at the initial stages. With time and increasing pH value, the peak becomes less broad and more symmetric. However, for the mixed solution of pH $\approx$ 6.8, the peak remains quite broad and asymmetric with time. This suggests that the initially formed AuNPs have either a large size distribution or chain-like aggregation or both. With time and increasing pH value, however, spherical AuNPs with a narrow size distribution and less aggregation, are formed. For the mixed solution of pH $\approx$ 6.8, no appreciable peak near 284 nm is observed at any time. The peak becomes visible with time as the pH value of the solution increases and becomes prominent for pH $\approx$ 10.6. Above this pH value, a visible peak near 284 nm is observed initially and remains almost unchanged with time. A prominent peak near 325 nm is observed for solutions with low pH values at the initial stages, due to the LMCT complex, which becomes weak and disappears with time and increasing pH value. Instead, a peak near 365 nm appears with time for high pH value solutions. The signature of the peaks (near 325 nm and 365 nm) and their evolution with time for solutions with different pH values are clear from the magnified view of the UV-vis spectra near that region, as shown in Fig. 4. An increase in the intensity of the plateau-like region (near 380–460 nm) with time is also observed, which is mainly related to the increase in the total number of gold atoms in the solution, irrespective of their form.[44,45]

To get further understanding of the growth of AuNPs, the evolution of the absorption intensity at 226, 284, 325, 365 and 460 nm and the SPR peak with time for the mixed ternary solutions of different pH values is plotted in Fig. 5. The intensity at 226 nm and the SPR peak were found to decrease and increase, respectively, with time, which was also obvious from the nature of the peaks and is expected. However, the intensities at 284 nm and 365 nm are found to increase, which was not obvious from the nature of the peaks and is not expected. Similarly, the intensity at 325 nm, which is found to first increase and then decrease or gradually increase with time, is not consistent with the nature of the peak or expectation. Such inconsistency is due to the evolution of the intensity near the plateau-like region (shown by the variation of the intensity at 460 nm) with time, which sometimes overshadowed the actual peak intensity. To get the actual peak variation, the contribution corresponding to the plateau-like region needs to be suppressed. The evolution of the relative intensity at 226, 284, 325 and 365 nm and the SPR peak (*i.e.* intensity relative to the intensity at 460 nm) with time for the mixed ternary solutions of different pH values is shown in Fig. 6. It is clear from this figure that the intensity corresponding to both the $AuCl_4^-$ ion (226 nm) and the LMCT complex (325 nm) decreases, while that of the SPR of the AuNPs ($I_{SPR,r}$) increases with time. The variation of $I_{SPR,r}(t)$ can be expressed quantitatively using standard exponential dependence,[46] namely $I_{SPR,r}(t) = I_{SPR,s}[1 - \exp(-t/\tau)]$, where $I_{SPR,s}$ is the saturation intensity and τ is the critical growth time. Analyzed curves using the above expression have been plotted in Fig. 5. The parameters $I_{SPR,s}$ and τ obtained from the analysis for different pH values are tabulated in Table 1. For the solution of pH $\approx$ 6.8, the peak intensity at 226 nm decreases sharply up to about 90 min and then nearly saturates, while that at 325 nm decreases slowly. The intensity at the SPR of the AuNPs increases moderately up to $\tau \approx$ 90 min. For the solution of pH $\approx$ 8.3, the sharp fall of the peak intensity at 226 nm takes place much earlier (before 60 min) and the decrease in the peak intensity at 325 nm is relatively fast, while the intensity at the SPR of the AuNPs increases relatively fast up to $\tau \approx$ 60 min. For the solution of pH $\approx$ 9.5, the intensity of both of the peaks (at 226 and 325 nm) is initially small, and decreases gradually then saturates. However, the intensity at the SPR of the AuNPs increases significantly up to $\tau \approx$ 50 min. For the solution of pH $\approx$ 10.6, the decrease in the intensity (at 226 and 325 nm) is slightly fast, while the increase in the intensity (at the SPR of the AuNPs) is very low up to $\tau \approx$ 40 min. For the solution of pH $\approx$ 11.2, the intensity of both the peaks (at 226 and 325 nm) is initially small, and decreases very fast and saturates within 20 min, while the intensity at the SPR of the AuNPs increases fast up to $\tau \approx$ 35 min. For the solution of pH $\approx$ 11.6, the behavior is similar to that of pH $\approx$ 11.2. However, the increase in the intensity (at the SPR of the AuNPs) is higher and increases quickly up to $\tau \approx$ 30 min. The intensity of the peak at 284 nm remains almost unchanged with time for all the solutions, with the exception of pH $\approx$ 10.6, where it first increases with time and then saturates. The intensity of the peak at 365 nm remains nearly the same or decreases slightly with time for most of the solutions, with the exception of the solutions with high pH values, for which the peak increases after some time. For the solution of pH $\approx$ 10.6, a small increase takes place after 60 min but the final value is less than that of the initial one, while for pH $\approx$ 11.2 and 11.6, an increase takes place after 20 min and the final value is relatively high. At the initial stages, the intensity of the peaks at 226 and 325 nm decreases considerably with increasing pH value, while that of the SPR peak of the AuNPs does not increase to such an extent. Rather, the intensity at 460 nm (*i.e.* for the plateau-like region) increases appreciably. In the final stages, the intensity of the SPR peak of the AuNPs first increases gradually with increasing pH value up to 9.5, then decreases suddenly and again increases a little bit with increasing pH value. The large decrease in the intensity for the solutions with high pH values is mainly counterbalanced by the increase in the intensity at the plateau-like region and at

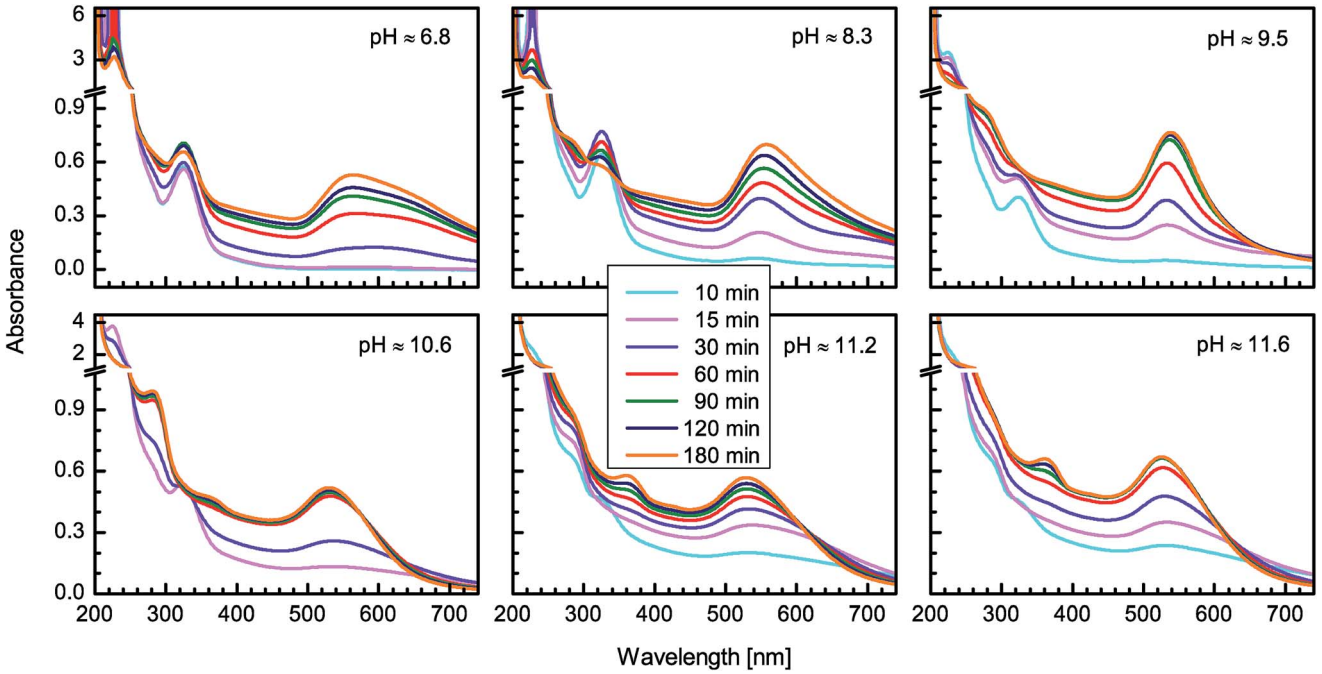

Fig. 3 Time-evolution UV-vis absorption spectra of the mixed ternary ($HAuCl_4$ + P123 + water) solutions of different pH values.

365 nm, while for the solution of pH ≈ 10.6, the increase in the intensity only occurs at 284 nm.

3.3 Transmission electron microscopy

Typical TEM images, at different resolutions, for the samples prepared from the mixed ternary ($HAuCl_4$ + P123 + water) solutions of different pH values are shown in Fig. 7. Formation of isolated AuNPs (dark spots), free P123 micelles (lighter spots) and small AuNP loaded large P123 micelles or micellar assemblies (dark spots in lighter contrast) are evident in the TEM images. However, the size of the isolated AuNPs is found to vary significantly with the pH value. The particle size distribution histograms for the isolated AuNPs and their average sizes

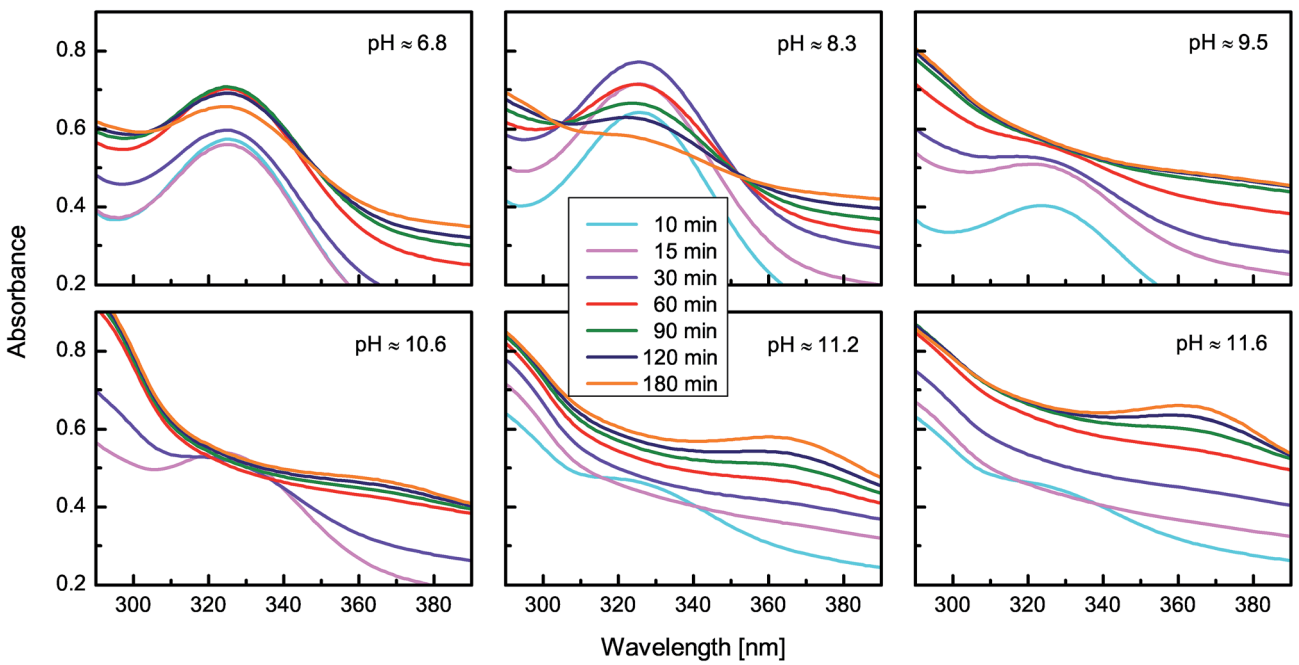

Fig. 4 Magnified view of the time-dependent UV-vis absorption spectra near 325 nm of the mixed ternary ($HAuCl_4$ + P123 + water) solutions of different pH values.

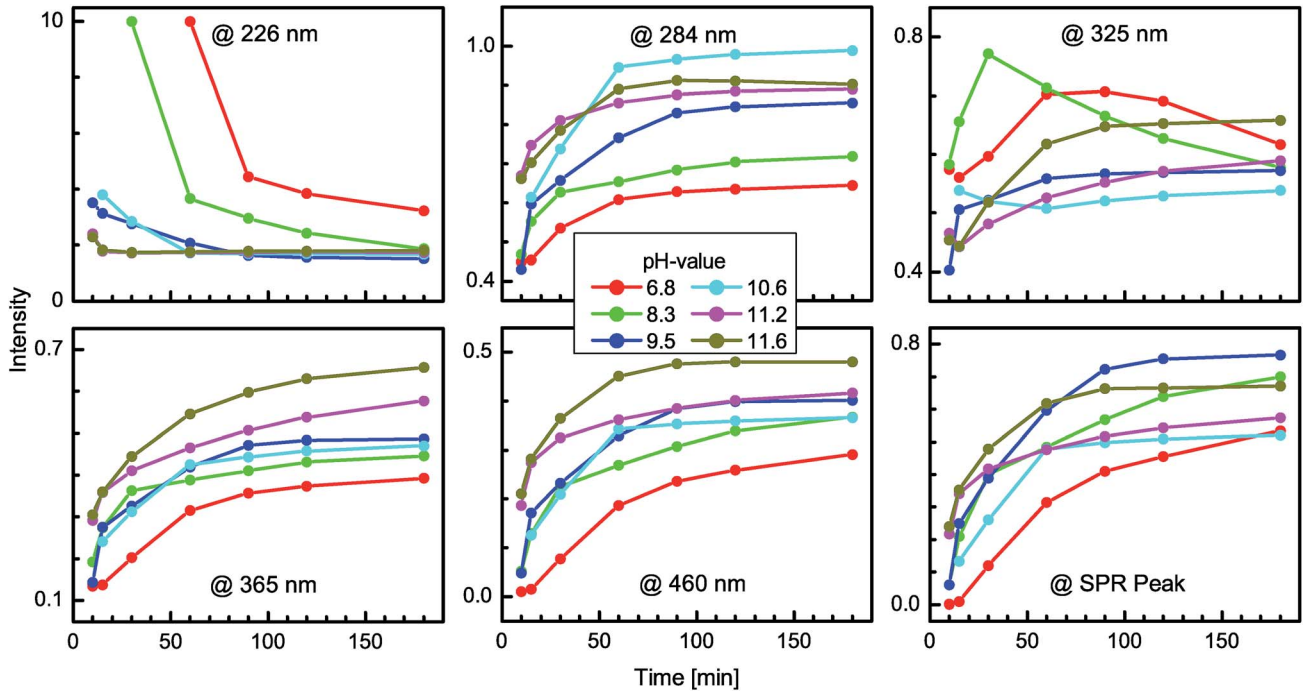

Fig. 5 Evolution of the absorption intensity at 226, 325, 365, 284 and 460 nm and the SPR peak with time for the mixed ternary ($HAuCl_4$ + P123 + water) solutions of different pH values.

($2R_{TEM}$), as obtained from the log-normal distribution for the mixed solutions of different pH values are shown in the insets of Fig. 7 and are also tabulated in Table 1. The formation of AuNPs or gold nanocrystals is further confirmed from the selected area diffraction pattern, as shown in Fig. 7d. For the sample prepared from the solution of pH ≈ 6.8, the average size of the AuNPs is found to be well-faceted, relatively large (about 49 nm), less uniform and slightly interconnected (see Fig. 7a–c). In the same sample the presence of free P123 micelles (of size about 19 nm) is also obvious, along with isolated AuNPs (see Fig. 7b). For the samples prepared from the solutions of pH ≈ 9.5, 10.6 and 11.6 (see Fig. 7e–g, i–k, m and n), the average sizes of the isolated AuNPs are found to be 16, 14 and 11 nm, respectively, which are quite small. Also the presence of free P123 micelles is

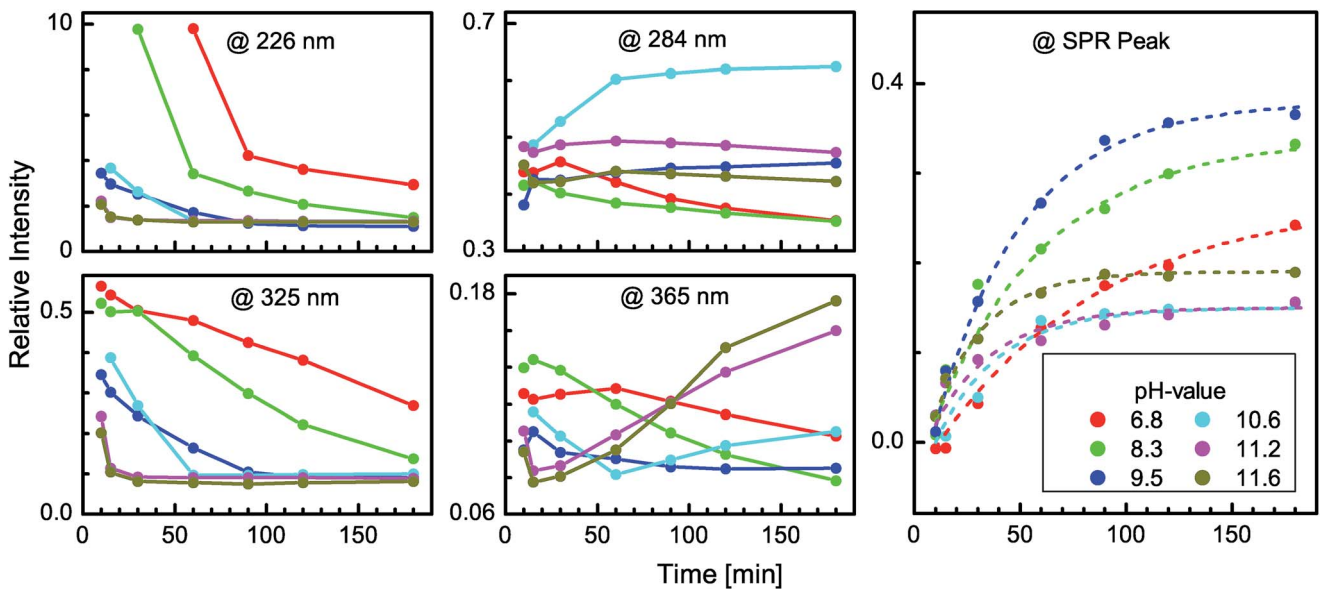

Fig. 6 Evolution of the absorption intensity at 226, 284, 325 and 365 nm and the SPR peak (relative to the intensity at 460 nm) with time for the mixed ternary ($HAuCl_4$ + P123 + water) solutions of different pH values. Solid lines through the data are to guide the eye, while dashed lines through the data are the analyzed curve.

observed (see Fig. 7e) in these samples. Additionally, very small AuNPs (less than 4 nm) incorporated into large P123 micelles are also observed in these samples, which are not found in the sample of pH ≈ 6.8.

It can be noted that the observed TEM results support well the findings of both the DLS and UV-vis studies. As predicted from the DLS and UV-vis results, the TEM results confirmed the formation of isolated AuNPs, the average size of which decreases with the increasing pH value, with a transition around pH ≈ 9.5. Below and above this pH value, the sizes of the isolated AuNPs are relatively big and small, respectively. However, the size estimated from TEM ($2R_{TEM}$) is less than that estimated from DLS ($2R_{DLS}$) and can be understood as follows. The size that we observed in the DLS measurements is the hydrodynamic diameter. So, it can overestimate the size due to the polymer coating and/or chain-like aggregation. The large objects of $2R_{DLS} > 100$ nm, for the low pH values, are probably due to such chain-like connectivity, as the TEM images show the formation of AuNPs of $2R_{TEM} \approx 49$ nm with some connectivity and the optical absorption spectra also show the asymmetric shape of the SPR peak. The overestimation of the small object of $2R_{DLS} \approx 19$ nm, for the high pH values, is probably due to the polymer coating. Additionally, the very small AuNPs, found to be incorporated into large P123 micelles for high pH values (from the TEM images) suggest that, at high pH values, not all Au ions form isolated AuNPs after reduction. Rather, some remain very small and are trapped in the micelles and some even stay in the near atomic states. Accordingly, in the UV-vis spectra, the intensity of the SPR peak is found to be relatively lower and the intensity near 460 nm or 365 nm is found to be relatively high.

3.4 Formation and growth of AuNPs in TBP solution

The results clearly show that the pH value of the P123 micellar solution has a significant influence on the reduction rate of the gold ions, the growth and stabilization of the AuNPs and on the final self-assembly of the nanoparticle–micelle nanocomposite. This is schematically illustrated in Fig. 8. In order to understand this in detail, let us first discuss the proposed formation mechanism of the AuNPs from the mixed aqueous solution of the gold salt and the TBP micelles in a single step synthesis process.

Generally, the strong tetrachloroauric(III) acid totally dissolved in aqueous solution generating $AuCl_4^-$ complex ions of square planar geometry and producing two absorption bands at 226 and 315 nm in the UV-vis absorption spectra corresponding to the $p_\sigma \rightarrow 5d_{x^2-y^2}$ (*i.e.* $\sigma \rightarrow \sigma^*$) and $p_\pi \rightarrow 5d_{x^2-y^2}$ (*i.e.* $\pi \rightarrow \sigma^*$) LMCT transitions, respectively.[47] The first of these is quite strong compared to the second one. It was reported earlier that, in aqueous solution, this $AuCl_4^-$ ion undergoes a pH-dependent step-wise hydrolysis, in which the replacement of chloride by hydroxide ligands takes place and the formation of the $[AuCl_x(OH)_{4-x}]^-$ complex ion occurs.[27,41,42,48] Accordingly, both the absorption bands were found to shift toward the lower wavelength value with the increase of the pH value.[27,41,42,48] However, in this study, no such shift is found. In fact, only the relatively strong lower wavelength band is observed, which remains fixed at 226 nm, indicating the formation of only $AuCl_4^-$ ions and no $[AuCl_x(OH)_{4-x}]^-$ complex ions even at high pH values. Thus it is clear that, unlike the high pH value of the aqueous solution of the gold salt, the high pH value of the aqueous P123 solution does not convert the $AuCl_4^-$ ions to $[AuCl_x(OH)_{4-x}]^-$ complex ions.

On the other hand, the TBP monomers, above the critical micelle concentration (cmc), aggregate in the aqueous solution to form well-defined micelles. The corona of the TBP micelle is composed of hydrophilic PEO units arranged in the form of surface cavities (a pseudo-crown ether structure) which can bind the $AuCl_4^-$ ions and act as sites for the site-specific redox reaction because of the presence of ether oxygen atoms.[5,12] The redox reaction, involving the reduction of $AuCl_4^-$ ions and the oxidation of the oxyethylene and oxypropylene segments of the TBP micelles initiates the synthesis of the nucleating centers of the AuNPs in the PEO–PPO–PEO surface cavities. The nucleating centers then undergo the growth process to produce AuNPs.[21,25] There are several processes for the growth of low dimensional structures in general.[3,7,25,49–52] The formation of AuNPs in solution, in the presence of sodium borohydride, is proposed to proceed through the rapid conversion of the ionic gold precursor into metallic gold nuclei, followed by particle growth *via* coalescence of smaller entities.[51] Growth of AuNPs in the presence of TBP micelles may occur between nucleating centers occupying neighboring surface cavities or through autocatalytic thermodynamically controlled reduction (ATCR), or both depending upon the micelle environment and the size and shape of micellar assemblies.[17–19] It should be noted that the formation of nanoparticles in solution can occur through LaMer nucleation, the Finke–Watzky two step mechanism, Ostwald ripening, digestive ripening, coalescence and orientated attachment, and intraparticle growth.[52] However, the prediction of the nanoparticle formation mechanism is still questionable, as a small change in the reaction conditions can lead to a completely different mechanism.[52]

Here the micellar solutions of high pH values (pH ≥ 6.8, *i.e.* toward the basic region) are prepared first and then the aqueous gold solution is mixed in and the aqueous gold solutions of high pH values are not prepared directly. In such conditions the high pH values do not convert the $AuCl_4^-$ ions into $[AuCl_x(OH)_{4-x}]^-$ complex ions and the appearance of the band at 325 nm is not due to the shift of the 315 nm band, rather it is due to the $AuCl_4^-$ ions binding with the PEO chains in the surface cavities. The pH value of the micellar solution strongly influences the reduction of the $AuCl_4^-$ ions and thus the nucleation and subsequent growth process to produce stable AuNPs with a narrow size distribution and well-defined morphology. When the pH value of the solution is low (here about 6.8) then the conversion of the $AuCl_4^-$ ions to Au atoms [*i.e.* reduction of Au(III) to Au(0)] after binding with the PEO chains of the surface cavities [*i.e.* Au(I)] is relatively slow and incomplete. Such a slow process seems to create less Au(0) nucleation centers, which then grow slowly, but enough, through the ATCR of gold ions on the surface of available nucleating centers that are present in the surface cavity of the micelle, and subsequently through

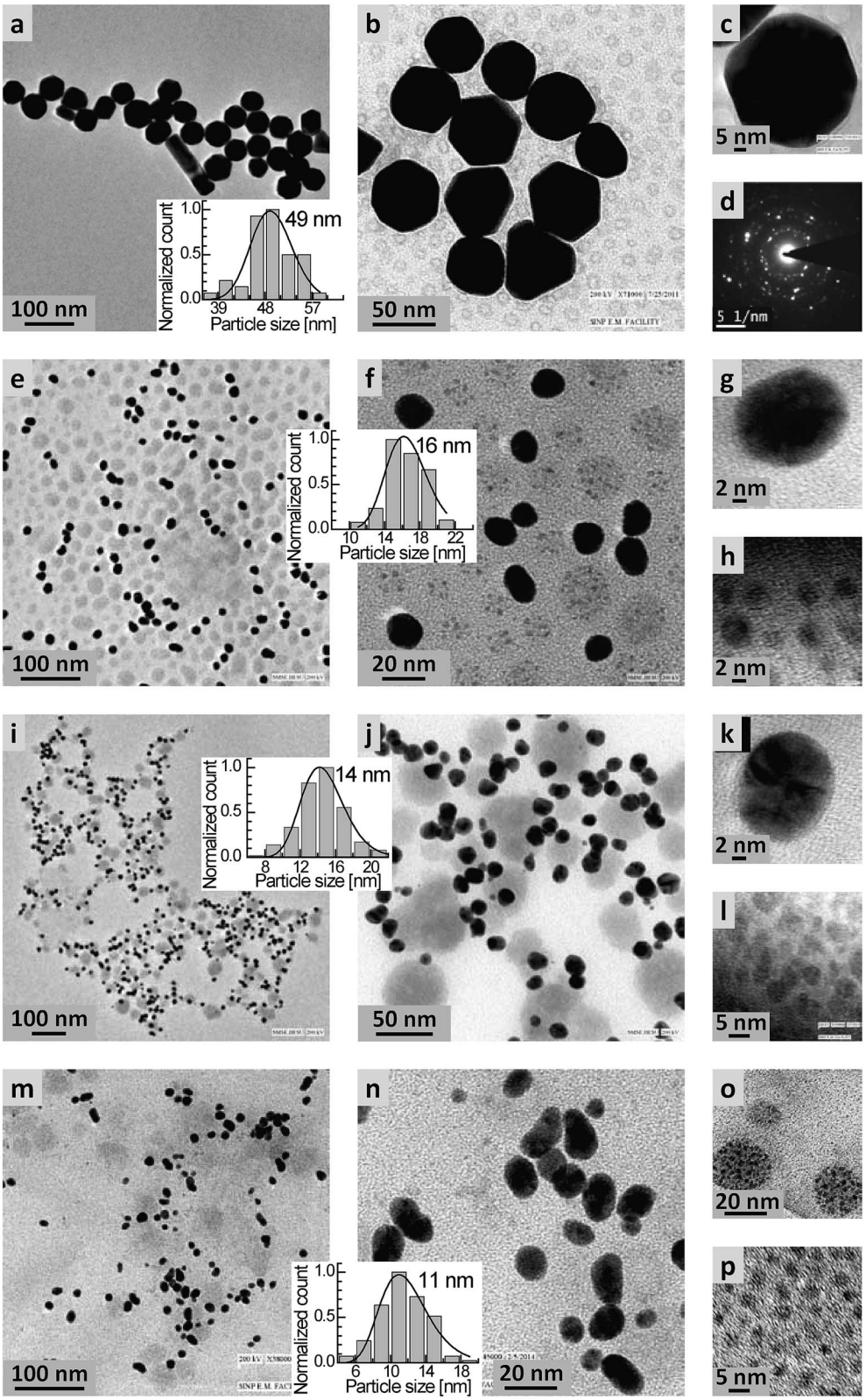

Fig. 7 Typical TEM images in different resolutions and a selected area diffraction pattern showing the formation of isolated AuNPs and also of small AuNP loaded large P123 micelles in the mixed ternary ($HAuCl_4$ + P123 + water) solutions of different pH values: (a)–(d) for pH ≈ 6.8, (e)–(h) for pH ≈ 9.5, (i)–(l) for pH ≈ 10.6 and (m)–(p) for pH ≈ 11.6. Insets: corresponding size histograms of isolated AuNPs and their average sizes, as obtained from log-normal distributions.

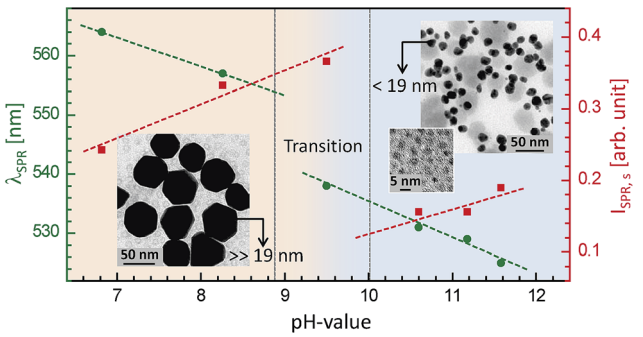

Fig. 8 Schematic illustration of the pH-dependent size and structural transition in P123 micelle induced AuNPs, showing a transition around pH ≈ 9.5 from slowly grown, well-faceted, large (≫19 nm), less uniform and near connected to fast grown, near symmetrical, small (<19 nm), more uniform and well separated AuNPs, and also a few trapped very small (<4 nm) AuNPs.

diffusion and coalescence to create relatively large and well-faceted AuNPs of different shapes, which can not be supported by the soft, small micelles. The initially formed AuNPs have chain-like aggregations of different chain lengths which, with time, grow to form more symmetrical and relatively large stable AuNPs of sizes much greater than that (about 19 nm) of the free micelles. As the pH value of the solution increases, the reaction rate and the conversion become fast and nearly complete. Accordingly, the number of nucleation centers increases, while the growth of the centers is restricted by the limited amount of available gold ions for further ATCR on one hand and interplay between the metal–polymer hydrophobic and polymer–water hydrophilic interactions on the other hand (to optimize the entropy and the free energy of the solution). Above the transition pH value (≈9.5) this restriction seems to be prominent. As a result, the controlled growth of the centers takes place through ATCR and diffusion followed by early capping through near individual micelles to form isolated symmetric small AuNPs of sizes less than that (about 19 nm) of the free micelles, with a narrow size distribution. The size of such AuNPs further decreases slowly with the increase of the pH value due to the increase of the reaction rate and hence the number of nucleation centers. Although, from our recent study, it is very difficult to favour a particular growth mechanism, nonetheless, from different experimental evidence and also considering the shape of the size distribution, it can be inferred that the growth is through ATCR, diffusion and coalescence. The diffusion is dominant in the initial phases and is prominent for the high pH values (where the growth is fast and the capping takes place early), while the coalescence is dominant in the latter stages and is prominent for the low pH values (where the growth is slow and takes place over a relatively long time).

It can be noted that at high pH values, although the conversion of $AuCl_4^-$ ions to Au atoms is fast and nearly complete (as observed from the optical absorption intensity at 226 and 325 nm), not all the Au atoms grow to form isolated AuNPs (as observed from the SPR peak intensity), though the majority do. Rather, the faster reduction rate of gold ions and simultaneous complete conversion of the LMCT complex to Au(0), produce a large number of nucleating centers within the surface cavity of the micelle and promote intermicelle fusion to produce some hybrid micelles of larger sizes. The surface cavity of the micelle acts as a soft template to form very small AuNPs (of sizes less than 4 nm) by entrapping some of the nucleating centers in its micellar phase (as observed from the optical absorption intensity at 365 and 460 nm and also from TEM images of very small AuNPs trapped in micellar assemblies). It is necessary to mention that above the transition pH value, isolated AuNPs of small sizes (less than 19 nm) with a narrow size distribution are formed, but at the same time there remains a significant amount of gold of very small sizes after reduction (formed in the early stages) that is trapped inside the micellar assemblies and/or in the near atomic states, which is of real concern and needs further study to improve the yield of the isolated small AuNPs by reducing the amount of such trapped and near atomic state gold.

4 Conclusions

The role of the pH value of the aqueous solution of P123 micelles in the growth and formation of AuNPs, in a single-step synthesis process, was evaluated using time-evolution UV-vis spectroscopy, DLS and TEM techniques. The basic medium of the P123 micelles converts the $AuCl_4^-$ ions to Au atoms [*i.e.* reduction of Au(III) to Au(0)] after binding them to the PEO chains of the surface cavities [*i.e.* Au(I)]. Initially converted Au atoms then act as nucleation centers, which subsequently grow through the ATCR of gold ions on the surface of available nucleating centers, diffusion and/or coalescence to form stable AuNPs. However, the conversion or reduction rate is found to depend strongly on the pH value, which essentially controls the growth of the AuNPs. For a pH value less than 9.5, the reduction rate is slow and the number of nucleation centers formed is lower. These, through subsequent ATCR, diffusion and coalescence, formed well-faceted near symmetrical large AuNPs of sizes much greater than that of the free P123 micelles. For a pH value above 9.5, the reduction rate of the gold ions is fast and the number of nucleation centers is large. Controlled growth of the centers takes place through ATCR (of the limited amount of available gold ions) and diffusion followed by early capping with near individual micelles. Isolated symmetrical small AuNPs of sizes <19 nm with a narrow size distribution are formed by optimizing the entropy and the free energy of the solution having large numbers of nucleation centers due to fast reduction, and further growth through ATCR and the metal–polymer and polymer–water interactions. Additionally, a large number of nucleating centers within the surface cavity of the micelles also promotes intermicelle fusion to produce some hybrid micelles of larger sizes, where very small sized AuNPs are trapped. Such trapped AuNPs and/or the observed near atomic state Au which cannot grow further, limited the yield of the desired isolated small AuNPs.

Acknowledgements

The authors thank Prof. P. M. G. Nambissan and Ms Soma Roy for their help in UV-vis measurements, Prof. M. Mukherjee for extending the DLS facility and Mr Pulak Ray, Prof. N. R. Bandyopadhyay and CRNN, University of Calcutta for TEM measurements.

References

1 S. Chen, C. Guo, G.-H. Hu, J. Wang, J.-H. Ma, X.-F. Liang, L. Zheng and H.-Z. Liu, *Langmuir*, 2006, **22**, 9704.
2 X. Ji, X. Song, J. Li, Y. Bai, W. Yang and X. Peng, *J. Am. Chem. Soc.*, 2007, **129**, 13939.
3 B.-K. Pong, H. I. Elim, J.-X. Chong, W. Ji, B. L. Trout and J.-Y. Lee, *J. Phys. Chem. C*, 2007, **111**, 6281.
4 K. Rahme, F. Gauffre, J.-D. Marty, B. Payre and C. Mingotaud, *J. Phys. Chem. C*, 2007, **111**, 7273.
5 P. Alexandridis, *Chem. Eng. Technol.*, 2011, **34**, 15.
6 T. S. Sabir, D. Yan, J. R. Milligan, A. W. Aruni, K. E. Nick, R. H. Ramon, J. A. Hughes, Q. Chen, R. S. Kurti and C. C. Perry, *J. Phys. Chem. C*, 2012, **116**, 4431.
7 H. Koerner, R. I. MacCuspie, K. Park and R. A. Vaia, *Chem. Mater.*, 2012, **24**, 981.
8 E. C. Dreaden, A. M. Alkilany, X. Huang, C. J. Murphy and M. A. El-Sayed, *Chem. Soc. Rev.*, 2012, **41**, 2740.
9 K. Saha, S. S. Agasti, C. Kim, X. Li and V. M. Rotello, *Chem. Rev.*, 2012, **112**, 2739.
10 I. Ojea-Jiménez, X. López, J. Arbiol and V. Puntes, *ACS Nano*, 2012, **6**, 2253.
11 P. Zhao, N. Li and D. Astruc, *Coord. Chem. Rev.*, 2013, **257**, 638.
12 M. S. Bakshi, *Adv. Colloid Interface Sci.*, 2014, **213**, 1.
13 M. Brust, M. Walker, D. Bethell, D. J. Schiffrin and R. Whyman, *J. Chem. Soc., Chem. Commun.*, 1994, 801.
14 K. Torigoe and K. Esumi, *Langmuir*, 1992, **8**, 59.
15 R. A. Caruso, M. Ashokkumar and F. Grieser, *Langmuir*, 2002, **18**, 7831.
16 T. Ishii, H. Otsuka, K. Kataoka and Y. Nagasaki, *Langmuir*, 2004, **20**, 561.
17 T. Sakai and P. Alexandridis, *Langmuir*, 2004, **20**, 8426.
18 T. Sakai and P. Alexandridis, *Langmuir*, 2005, **21**, 8019.
19 P. Khullar, A. Mahal, V. Singh, T. S. Banipal, G. Kaur and M. S. Bakshi, *Langmuir*, 2010, **26**, 11363.
20 D. Ray, V. K. Aswal and D. Srivastava, *J. Nanosci. Nanotechnol.*, 2010, **10**, 6356.
21 P. Khullar, V. Singh, A. Mahal, H. Kaur, V. Singh, T. S. Banipal, G. Kaur and M. S. Bakshi, *J. Phys. Chem. C*, 2011, **115**, 10442.
22 S. Dey, A. Adhikari, U. Mandal, S. Ghosh and K. Bhattacharyya, *J. Phys. Chem. B*, 2008, **112**, 5020.
23 D. Ray, V. K. Aswal and J. Kohlbrecher, *Langmuir*, 2011, **27**, 4048.
24 S. Mandal, C. Ghatak, V. G. Rao, S. Ghosh and N. Sarkar, *J. Phys. Chem. C*, 2012, **116**, 5585.
25 T. Sakai and P. Alexandridis, *J. Phys. Chem. B*, 2005, **109**, 7766.
26 Q. Shou, C. Guo, L. Yang, L. Jia, C. Liu and H. Liu, *J. Colloid Interface Sci.*, 2011, **363**, 481.
27 S. Wang, K. Qian, X. Z. Bi and W. Huang, *J. Phys. Chem. C*, 2009, **113**, 6505.
28 W. P. Halperin, *Rev. Mod. Phys.*, 1986, **58**, 533.
29 P. Mulvaney, *Langmuir*, 1996, **12**, 788.
30 S. Link and M. A. El-Sayed, *J. Phys. Chem. B*, 1999, **103**, 8410.
31 S. Hazra, A. Gibaud and C. Sella, *Appl. Phys. Lett.*, 2004, **85**, 395.
32 S. Hazra, *Appl. Surf. Sci.*, 2006, **253**, 2154.
33 S. Hazra, A. Gibaud and C. Sella, *J. Appl. Phys.*, 2007, **101**, 113532.
34 W. Haiss, N. T. K. Thanh, J. Aveyard and D. G. Fernig, *Anal. Chem.*, 2007, **79**, 4215.
35 V. Amendola and M. Meneghetti, *J. Phys. Chem. C*, 2009, **113**, 4277.
36 I. Roy and S. Hazra, *Soft Matter*, 2015, **11**, 3724.
37 I. Roy and S. Hazra, *RSC Adv.*, 2015, **5**, 665.
38 W. Brown, *Dynamic Light Scattering: The Method and Some Applications*, Clarendon Press, Oxford, 1993.
39 B. J. Berne and R. Pecora, *Dynamic Light Scattering*, Dover Publications, New York, 2000.
40 A. Gibaud, S. Hazra, C. Sella, P. Laffez, A. Désert, A. Naudon and G. Van Tendeloo, *Phys. Rev. B: Condens. Matter Mater. Phys.*, 2001, **63**, 193407.
41 D. V. Goia and E. Matijevic, *Colloids Surf., A*, 1999, **146**, 139.
42 I. Ojea-Jiménez, F. M. Romero, N. G. Bastús and V. Puntes, *J. Phys. Chem. C*, 2010, **114**, 1800.
43 H. Isci and W. R. Mason, *Inorg. Chem.*, 1983, **22**, 2266.
44 C. F. Bohren and D. R. Huffman, *Absorption and Scattering of Light by Small Particles*, Wiley-Interscience, New York, 1983.
45 Y.-Y. Fong, J. R. Gascooke, B. R. Visser, G. F. Metha and M. A. Buntine, *J. Phys. Chem. C*, 2010, **114**, 15931.
46 P. Chatterjee and S. Hazra, *J. Phys. Chem. C*, 2014, **118**, 11350.
47 A. K. Gangopadhayay and A. Chakravorty, *J. Chem. Phys.*, 1961, **35**, 2206.
48 S. Ivanova, C. Petit and V. Pitchon, *Appl. Catal., A*, 2004, **267**, 191.
49 J. K. Basu, S. Hazra and M. K. Sanyal, *Phys. Rev. Lett.*, 1999, **82**, 4675.
50 J. K. Bal and S. Hazra, *Phys. Rev. B: Condens. Matter Mater. Phys.*, 2009, **79**, 155412.
51 J. Polte, R. Erler, A. F. Thünemann, S. Sokolov, T. T. Ahner, K. Rademann, F. Emmerling and R. Kraehnert, *ACS Nano*, 2010, **4**, 1076.
52 N. T. K. Thanh, N. Maclean and S. Mahiddine, *Chem. Rev.*, 2014, **114**, 7610.